Microwave emission from density-stratified Antarctic firn at 6 cm wavelength

RICHARD D. WEST

Department of Electrical Engineering, University of Washington, Seattle, Washington 98195, U.S.A.

DALE P. WINEBRENNER

Applied Physics Laboratory, University of Washington, Seattle, Washington 98195, U.S.A.

LEUNG TSANG

Department of Electrical Engineering, University of Washington, Seattle, Washington 98195, U.S.A.

HELMUT ROTT

Institut für Meteorologie und Geophysik, Universität Innsbruck, A-6020 Innsbruck, Austria

ABSTRACT. Previous observations have shown spatial covariances between microwave emission from Antarctic firn at 6 cm wavelength, physical firn temperature and firn-density stratification. Such observations motivate us to understand the physics underlying such covariances and, based on that understanding, to develop estimation methods for firn temperature and layering parameters. We present here a model for 6 cm emission from firn in which density, and therefore dielectric permittivity, varies randomly in discrete layers with mean thicknesses on the order of centimeters. The model accounts for depth profiles of the physical temperature, mean density and variance of random density fluctuations from layer to layer. We also present a procedure to estimate emission-model input parameters objectively from in situ density-profile observations, as well as uncertainties in the input parameters and corresponding uncertainties in theoretical brightness-temperature predictions. We compare emission-model predictions with ground-based observations at four diverse sites in Antarctica which span a range of accumulation rates and other parameters. We use coincident characterization data to estimate model inputs. At two sites, layered-medium emission-model predictions based on the most probable input parameters (i.e. with no model tuning) agree with observations to within 3.5% for incidence angles ≤50°. Corresponding figures for the other two sites are 7.5% and 10%. However, uncertainties in the input parameters are substantial due to the limited length and depth resolution of the characterization data. Uncertainties in brightness-temperature predictions are correspondingly substantial. Thus brightness-temperature predictions for the last-mentioned sites based on only slightly less probable input parameters are also in close agreement with observations. The significance of agreements and discrepancies could be clarified using characterization measurements with finer depth resolution.

INTRODUCTION

Microwave emission from Antarctic firn has recently been shown to be correlated with mean annual temperatures and snow-accumulation rates (Zwally, 1977; Rotman and others, 1982; Fily and Benoist, 1991; Surdyk and Fily, 1993). In particular, vertically polarized emission near 6 cm wavelength correlates strongly with physical temperature (Fily and Benoist, 1991), while the corresponding horizontally polarized emission is affected by the amount of stratification (Surdyk and Fily, 1993). Horizontally polarized emission at short wavelengths (1.6 and 0.8 cm) is also evidently affected by surface hoar and snow density in the first few centimeters of the surface

(Shuman and others, 1993). Remote estimation of these variables would be valuable in studies of the dynamics and thermodynamics of the Antarctic ice sheet. These considerations strongly motivate a better understanding of how firn structure affects microwave emission.

Recent studies by Rott in east Antarctica resulted in firn-characterization data and coincident microwave-emission observations at 6 and 3 cm wavelengths at several sites (Rott and others, 1993a, b). The polar firn at these sites, as elsewhere (Benson, 1959; Alley, 1988), displayed numerous layers of differing density on the order of centimeters in thickness. Boundaries between adjacent layers were relatively sharp, i.e., the transition between layers occurred over depth intervals much less

than the typical layer thickness. Typical layer thicknesses, mean firn density, the variance in density from layer to layer, and microwave emission all varied considerably between sites.

Individual layers of polar firn differ from each other in grain-size distribution, texture, density, isotopic concentrations and other properties. These properties are of interest in many geophysical studies, but only those properties that affect microwave scattering are germane to this study. In general, electromagnetic scattering depends on the detailed dielectric structure of the firn. Microwave scattering in particular is sensitive to two types of dielectric discontinuities, volume inhomogeneities such as ice grains, and abrupt changes in dielectric constant at interfaces between layers with differing densities (Mätzler, 1987).

Theoretically computed microwave emission from homogeneous (i.e. non-layered) firn with the observed mean densities differs considerably from 6 cm wavelength observations (see below). The predicted brightness temperatures exceed those observed, while the predicted difference between vertically and horizontally polarized emission is much smaller than that observed. Previous work (Zwally, 1977; Cosimo and others, 1982; Surdyk and Fily, 1993) has shown that scattering from individual ice particles is important at short wavelengths (e.g. 0.8 and 1.6 cm). At longer wavelengths (e.g. 6 and 3 cm), calculations based on scattering from individual ice particles in the firn do not accurately reproduce the characteristics of available data (unpublished computations by R. West, D. Winebrenner and L. Tsang). However, it is known that scattering from layers similar to those observed in firn can significantly lower brightness temperatures (from those in the corresponding homogeneous-firn case) and increase the difference between vertically and horizontally polarized emission (Tsang and others, 1987).

Thus, in this paper we study the effect of stratification of firn density on microwave emission at 6 cm wavelength using signature modeling and Rott's data set. We restrict ourselves in this initial study to 6 cm wavelength because we want to minimize possible effects of scattering from individual ice grains and thereby gain a clearer understanding of stratification effects alone. We will extend the present study to include grain-scattering effects at shorter wavelengths in a forthcoming study.

The paper is divided into three major sections. First, we introduce a model for the layered structure of firn motivated by direct observations, and describe objective statistical procedures to estimate model parameters from the available characterization data. We discuss a rigorous layered-medium emission model based on Maxwell's equations and fluctuation–dissipation theory. This model is used to compute theoretical brightness temperatures that depend on the physical-temperature profile and scattering from interfaces between firn layers of different densities. In the penultimate section, we apply the statistical procedures to characterization data, and use the emission model to compute theoretical brightness temperatures. We describe a procedure to estimate quantitatively the uncertainties in parameters used as input to the emission model and the resulting uncertainties in predicted brightness temperatures. In the final section, we draw conclusions from the results.

A MODEL FOR LAYERED ANTARCTIC FIRN

A number of investigators have described discrete layering on centimeter scales in polar firn (Benson, 1959; Alley, 1988; Rott and others, 1993b). For example, the solid line in Figure 1 shows the density profile at Rott's Veststraumen site (Rott and others, 1993b). The density measurements were made by extracting and weighing successively deeper firn sections of known volume. The vertical extent of each section was 5 cm and the centers of successive sections were 5 cm apart. The result is an averaged density profile. The averaging obscures the underlying density profile somewhat; direct qualitative observations indicated that some physical layers and crusts were actually thinner than 5 cm. We provide information on glaciological and other parameters at this site in the section on comparison of theory with observations.
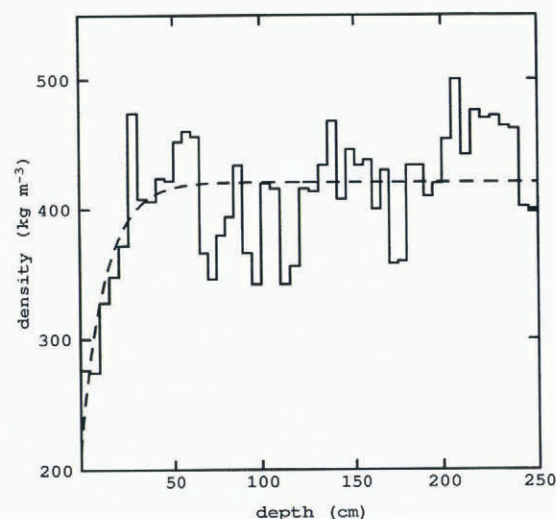

Fig. 1. The snow-density profile at Veststraumen (solid line). The profile was obtained by measuring the average density in consecutive 5 cm layers. The dashed line shows the least-squares exponential fit to the measured profile. The fitted exponential is: $F(z) = 421 - 206 \exp(7.8z)$ with z a negative value in meters, and $F(z)$ measured in $kg\,m^{-3}$.

In Figure 1, we see a non-linear trend in the mean density as a function of depth. The trend is most pronounced near the surface, and is also observed at other sites (Rott and others, 1993b). Although it is not visible in Figure 1, other studies of the depth independence of firn density (Benson, 1959; Gow, 1968) have shown a characteristic decrease in density variations with depth, and an increase in the mean density level. The decrease in density variation is most visible at depths greater than 4–5 m.

Firn layering is typically not horizontally coherent over length scales of more than a few meters (Benson, 1959; Alley, 1988, figs 2 and 3). Satellite-emission measurements cover a large footprint, and therefore represent an average over density profiles present inside the field of view of the radiometer. The ground-based radiometer measurements are also averaged over several

different density profiles at each site. To model this type of averaging, we first assume no horizontal variation in the layering, but then average results over several realizations.

Our model for density as a function of depth consists of a sum of a deterministic part, $F(z)$, and a stationary stochastic part, $X(z)$: $D(z) = F(z) + X(z)$. The deterministic function $F(z)$ models the non-linear trend apparent in the measured profile. Since the measured profile shows an apparent rise and saturation in mean level, we chose an exponential function for $F(z)$.

$$F(z) = a + b\exp(cz). \qquad (1)$$

The parameters a, b and c are determined by fitting $F(z)$ to the measured density profile in the least-squares sense. The dashed line in Figure 1 shows the exponential function fitted for the profile at Veststraumen. The primary importance of $F(z)$ is to "detrend" the density data. It is not related to the gradual densification of snow which occurs at depths greater than a few meters. The detrending allows a variety of statistical techniques to be used on the remaining centered stationary process $X(z)$. The scattering problem and computation of emission (described in the next section) are relatively insensitive to changes in $F(z)$ by itself. However, the presence of the non-linear mean density profile can slightly bias our estimates of other parameters. We discuss this issue further in the context of comparing the emission model with observations.

The stochastic process $X(z)$ describes the randomly layered structure in the upper few meters of firn. We form $X(z)$ from two single-parameter random processes, one describing the thicknesses of layers, the other describing the variation from the mean density in each layer. We assume that the thicknesses of layers are exponentially distributed with parameter λ (average layer thickness $= 1/\lambda$), and that the thickness of each layer is independent of the thicknesses of all other layers. Thus, the depth-of-layer interfaces form a Poisson sequence. We assume that the variation from the mean background density in each layer (determined by $F(z)$) is Gaussian-distributed with zero mean and a standard deviation σ. We further assume that the deviations from mean density are independent from layer to layer. The combination of these two random processes is similar to the random telegraph process described by Papoulis (1991, ch. 10). Using the methods described by Papoulis, we computed the autocorrelation function $R_{XX}(z_1, z_2)$ and the spectral-density function $S_X(\omega)$ of the stochastic process $X(z)$.

$$R_{XX}(z_1, z_2) = \sigma^2 e^{-\lambda|z_2 - z_1|}. \qquad (2)$$

$$S_X(\omega) = \frac{2\sigma^2\lambda}{\lambda^2 + \omega^2}. \qquad (3)$$

Our profile data are not statistically sufficient to test the validity of these assumptions; the test of their validity will be in the comparison of our combined firn-structure and emission models with observations. There are, however, some grounds for optimism based on theory, in that emission from random media slightly simpler than that

supposed here is theoretically insensitive to plausible variations in the distributions of layer densities (Klyatskin and Tatarskii, 1977).

Our model includes the observed decrease in density variations with depth, and the observed increase in mean background density (Benson, 1959; Gow, 1968). The standard deviation of the density variations, σ, is assumed to be constant in the top 4 m of firn. Starting at a depth of 4 m, σ is reduced as a linear function of depth until it reaches zero at a depth of 16 m. At 10 m depth, σ is half of its maximum value. Also starting at a depth of 4 m, the mean background density level is increased as a linear function of depth until it reaches a value of 600 kg m^{-3} at a depth of 16 m. This gives a density profile similar to that observed in the upper parts of ice cores from Antarctica and Greenland (Benson, 1959; Gow, 1968).

To estimate λ and σ objectively from characterization data, one might naively try to fit Equation (3), in the least-squares sense, to a spectral estimate for observed detrended density fluctuations. However, three effects complicate the situation. First, the spectral estimate includes the effects of a 5 cm moving average due to the characterization procedure. Secondly, the spectral estimate includes aliasing caused by the discrete sampling used to obtain the density data. Finally, the spectral estimate will include distortion and bias depending on the nature of the spectral estimator used. These effects cannot be removed from the estimated spectrum of the data (Percival and Walden, 1993, ch. 6). We therefore incorporate them into a modified spectral model which we can then fit to the characterization data directly.

The modified spectral model is formed by applying the three distorting effects to the stochastic process $X(z)$. The 5 cm moving average is equivalent to convolving $X(z)$ with a unit-square window of width 5 cm. Let $X_a(z)$ be the resulting moving-average process. The spectrum of $X_a(z)$ is the product of the spectrum of the window and the spectrum of $X(z)$.

$$S_{X_a}(\omega) = \frac{8\sigma^2\lambda \sin^2(\omega\frac{\Delta_d}{2})}{\Delta_d^2\omega^2(\lambda^2 + \omega^2)}. \qquad (4)$$

The quantity Δ_d in Equation (4) is the size of the moving average (in the present data, 5 cm). The standard deviation of the moving-average process, σ_a, is determined by evaluating the autocorrelation of $X_a(z)$ at zero lag. The autocorrelation of $X_a(z)$ at zero lag is just the inverse Fourier transform of $S_{X_a}(\omega)$ evaluated at $z = 0$. The result is a relationship between σ_a and σ.

$$\sigma_a^2 = 2\frac{\sigma^2}{\lambda^2\Delta_d^2}\left(\lambda\Delta_d - 1 + e^{-\lambda\Delta_d}\right). \qquad (5)$$

We use as our estimate for σ_a the standard deviation of the detrended density data.

The moving-average process $X_a(z)$ is now sampled at 5 cm intervals, giving a discrete process X_{an}. The finite sampling interval causes aliasing. Power at frequencies higher than the Nyquist frequency (10 cycles m^{-1} in this case) is aliased down into the range [0,10] cycles m^{-1} (Percival and Walden, 1993, ch. 4). The resulting spectrum is

$$S_{X_{\mathrm{an}}}(\omega) = \sum_{k=-\infty}^{\infty} S_{X_{\mathrm{a}}}\left(\omega + \frac{2\pi k}{\Delta_z}\right). \qquad (6)$$

The nature of the measurement process makes the sampling interval Δ_z equal to the size of the moving average Δ_{d}. Since $S_{X_{\mathrm{a}}}(\omega)$ rapidly decays to zero with increasing ω, the infinite sum in Equation (6) can be truncated after enough terms have been included to capture most of the power in the continuous spectrum $S_{X_{\mathrm{a}}}(\omega)$.

In this study, we chose the periodogram as the spectral estimator, so we must consider a few additional concerns raised by the nature of the periodogram. First, the theoretical spectrum should be scaled to match the normalization of the periodogram. Secondly, the finite length of the data makes it impossible for a periodogram to estimate the zero-frequency component; we therefore discard this component of the spectrum prior to the least-squares fit. Finally, the spectrum of the square window (implied by the finite length of the data record) can cause bias and distortion in a periodogram special estimate (Papoulis, 1991; Percival and Walden, 1993). However, the dynamic ranges of the firn spectra in this study are relatively low ($< 20\,\mathrm{dB}$), so a periodogram gives effectively unbiased results (Percival and Walden, 1993, ch. 6).

In practice, we apply the least-squares fit to the natural logarithm of the theoretical spectrum, $S_{X_{\mathrm{an}}}(\omega)$, and the natural logarithm of the periodogram of the data because the log spectrum has constant variance as a function of frequency; this property makes the fitting procedure more convenient. However, taking the logarithm of a periodogram introduces a bias relative to the logarithm of the theoretical spectrum (Percival and Walden, 1993, ch. 6). We correct for this effect by adding the known bias (Euler's constant) to the natural logarithm of the periodogram. Fitting the log spectrum gives an estimate of λ which can then be used with the estimate of σ_{a} and Equation (5) to obtain an estimate for σ. Figure 2 shows the logarithm of the estimated data spectrum and the fitted log theoretical spectrum for Veststraumen. The large scatter of the estimated data spectrum is due to the relatively short length of the data record, and leads to a relatively high uncertainty in the estimates of λ and σ. In the section discussing the observations, we present a method of estimating quantitatively the uncertainties in the parameter estimates, and the resulting variation in the theoretical brightness temperatures.

The estimates of λ and σ are used to generate many realizations of simulated Antarctic firn for use in subsequent brightness-temperature calculations. Note that the computation of brightness temperatures will be based on the underlying stochastic process $X(z)$, not the sampled moving-average process X_{an}. The moving average and sampling interval are artifacts of the measurement process used to obtain the density profile; they have nothing to do with the emission measurement or calculation. In the next section, we summarize a theory for microwave emission from the randomly layered physical model just described.
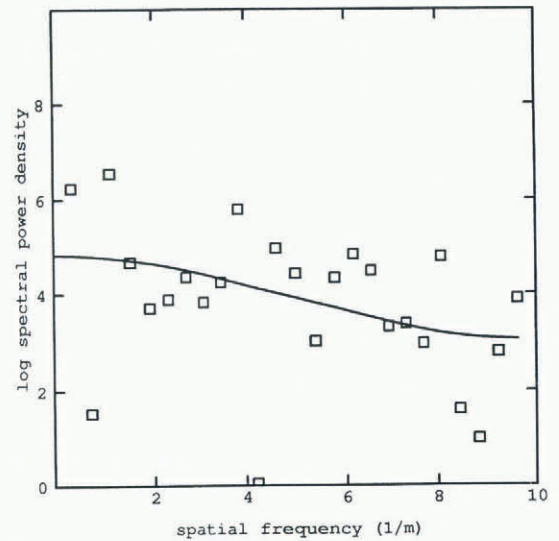

Fig. 2. A comparison between the natural logarithm of the periodogram for the measured density profile at Veststraumen (open squares) and the theoretical log spectrum (solid line) fitted in the least-squares sense with $1/\lambda = 3.10\,cm$, and $\sigma = 49.9\,kg\,m^{-3}$. The spectrum itself has units of $(kg\,m^{-3})^2/(1/m)$.

THERMAL EMISSION FROM A LAYERED MEDIUM

The problem in this section is to compute the brightness temperature of the stratified medium used to represent Antarctic firn. The physical model developed in the previous section is shown schematically in Figure 3. The model assumes homogeneous layers with planar interfaces. Region 0 is free space, while all the other layers consist of dry snow. Each layer is characterized by a density and a physical temperature which is constant inside the layer. The physical-temperature characterization data are fitted by an exponential function of the form $T(z) = T_0 + T_{\mathrm{h}}\exp(\gamma z)$. T_0 is the mean annual temperature encountered at 10 m depth, $T_0 + T_{\mathrm{h}}$ is the surface temperature, and γ is the temperature-decay rate as depth increases (z is 0 at the surface and negative inside the layered medium). The density profile is converted into a permittivity profile using the following empirical
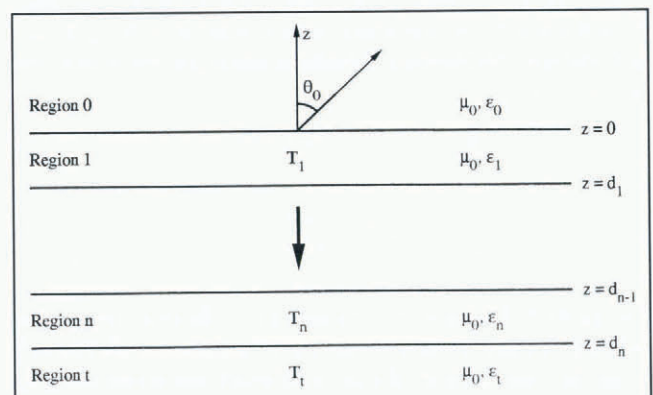

Fig. 3. The layered-medium model used to represent Antarctic firn.

mixing formula given by Mätzler (1987) for dry snow.

$$\epsilon' = 1 + \frac{1.60\rho}{1 - 0.35\rho}$$
$$\epsilon'' = \epsilon''_{\text{ice}}(0.52\rho + 0.62\rho^2)$$
$$\epsilon = \epsilon' + i\epsilon''. \qquad (7)$$

In the equation above, ρ is the snow density in g cm^{-3}, and $\epsilon''_{\text{ice}} = 0.00033$ is the imaginary part of the dielectric constant of pure ice at a frequency of 5.25 GHz and a temperature of $-15°$C (Mätzler, 1987). This quantity is treated as a constant over the range of temperatures in the profiles studied. In reality, there is a small change with temperature, but this is not large enough to cause a noticeable change in computed brightness temperatures. The imaginary part of the effective snow permittivity represents the small amount of attenuation in snow at microwave frequencies.

To determine the thermal emission of the stratified medium shown in Figure 3, we need to characterize the source of the emission, and solve Maxwell's equations for scattering in a one-dimensional geometry. A fully coherent field solution is used because the wavelength and layer thicknesses are comparable, and the scattering rate in each layer is small enough that reflected energy is not significantly randomized while propagating through one layer. This means that phase relationships between incident and reflected sources of intensity at a layer interface may be important enough to affect the calculation. In future work, we will compare these results with results obtained using an incoherent radiative-transfer solution. In the next several paragraphs, we summarize the important features of the coherent theory as they apply to layered Antarctic firn.

Thermal radiation from snow is caused by thermally induced movements of microscopic charges in the medium. This random motion of charges can be viewed as a randomly fluctuating equivalent current density. Let $\bar{J}_l(\bar{r}, \omega)$ be the equivalent thermal-current density in region l as a function of position and frequency. There is no net current, so the ensemble average is zero $(\langle \bar{J}_l(\bar{r}, \omega) \rangle = 0)$, but the expected value $(\langle \bar{J}_l(\bar{r}, \omega) \bar{J}_l^*(\bar{r}', \omega') \rangle$ is non-zero. The fluctuation–dissipation theorem (Callen and Welton, 1951; Landau and Lifshitz, 1960; Tsang and others, 1987) relates the equivalent current source with the physical temperature and lossy characteristics of the medium. Tsang and others (1987, ch. 2) summarize the derivation of the result

$$\langle \bar{J}_l(\bar{r}, \omega) \bar{J}_l^*(\bar{r}', \omega') \rangle = \frac{4}{\pi} \omega \epsilon_l'' KT_l \bar{\bar{I}} \delta(\omega - \omega') \delta(\bar{r} - \bar{r}'). \qquad (8)$$

K is Boltzmann's constant, T_l is the physical temperature in region l, $\bar{I}$ is the unit dyad, and ϵ_l'' is the imaginary part of the permittivity in region l. Equation (8) is valid as long as the Rayleigh–Jeans limit holds ($\bar{h}\omega << KT$, where $\bar{h}$ is Planck's constant) and local thermodynamic equilibrium applies. Both of these conditions are met by Antarctic snow at microwave frequencies. This result also assumes that the fluctuations of $\bar{J}_l(\bar{r}, \omega)$ are uncorrelated between neighboring volume elements (hence the term $\delta(\bar{r} - \bar{r}')$).

The next step is to compute the electromagnetic field generated by $\bar{J}_l(\bar{r}, \omega)$. According to Maxwell's equations (in time-harmonic form), the electric field satisfies the following vector-wave equation.

$$\nabla \times \nabla \times \bar{E}(\bar{r}, \omega) - \frac{\omega^2}{c^2} \bar{E}(\bar{r}, \omega) = i\omega\mu \bar{J}_l(\bar{r}, \omega). \qquad (9)$$

E is the electric field, c is the local speed of light in the medium, and μ is the magnetic permeability.

The solution of the wave equation can be expressed compactly in terms of a dyadic Green's function

$$\bar{E}(\bar{r}\omega) = i\omega\mu \int_V \bar{\bar{G}}(\bar{r}, \bar{r}') \bar{J}_l(\bar{r}', \omega)d\bar{r}'. \qquad (10)$$

Since the geometry of the problem is planar, the dyadic Green's function for a stratified medium is used. The radiated intensity and brightness temperature are then related to the correlation of the field. Tsang and others (1987, ch. 2) apply a propagation-matrix formulation to this problem and obtain a solution for the vertically and horizontally polarized brightness temperatures in a form easily solved on a computer.

$$T_{\text{Bh}}(\theta_0) = \frac{k}{\cos\theta_0} \frac{\epsilon_t'' T_t}{2\epsilon_0 k_{tz}''} |B_t|^2 e^{-2k_{tz}'' d_n}$$
$$+ \frac{k}{\cos\theta_0} \sum_{l=1}^n \frac{\epsilon'' T_l}{2\epsilon_0} \left\{ \frac{|A_l|^2}{k_{lz}''} (e^{2k_{lz}'' d_l} - e^{2k_{lz}'' d_{l-1}}) \right.$$
$$- \frac{|B_l|^2}{k_{lz}''} (e^{-2k_{lz}'' d_l} - e^{-2k_{lz}'' d_{l-1}})$$
$$+ \frac{i A_l B_l^*}{k_{lz}'} (e^{-i2k_{lz}' d_l} - e^{-i2k_{lz}' d_{l-1}})$$
$$\left. - \frac{i A_l^* B_l}{k_{lz}'} (e^{i2k_{lz}' d_l} - e^{i2k_{lz}' d_{l-1}}) \right\}. \qquad (11)$$

$$T_{\text{Bv}}(\theta_0) = \frac{k}{\cos\theta_0} \frac{\epsilon_t'' T_t(|k_{tz}|^2 + k_x^2)}{2\epsilon_0 k_{tz}'' |k_t|^2} |D_t|^2 e^{-2k_{tz}'' d_n}$$
$$+ \frac{k}{\cos\theta_0} \sum_{l=1}^n \frac{\epsilon'' T_l(|k_{lz}|^2 + k_x^2)}{2\epsilon_0 |k_l|^2}$$
$$\cdot \left\{ \frac{|C_l|^2}{k_{lz}''} (e^{2k_{lz}'' d_l} - e^{2k_{lz}'' d_{l-1}}) \right.$$
$$- \frac{|D_l|^2}{k_{lz}''} (e^{-2k_{lz}'' d_l} - e^{-2k_{lz}'' d_{l-1}})$$
$$+ \frac{|k_{lz}|^2 - k_x^2 C_l D_l^*}{|k_{lz}|^2 + k_x^2 i k_{lz}'} (e^{-i2k_{lz}' d_l} - e^{-i2k_{lz}' d_{l-1}})$$
$$\left. - \frac{|k_{lz}|^2 - k_x^2 C_l^* D_l}{|k_{lz}|^2 k_x^2 i k_{lz}'} (e^{i2k_{lz}' d_l} - e^{i2k_{lz}' d_{l-1}}) \right\}. \qquad (12)$$

We assume that the plane of observation is the xz-plane, so $k_y = 0$. In the two equations above we use: $k_l = k_l' + ik_l'' = \omega\sqrt{\epsilon_l\mu}$, where ϵ_l is the permittivity of layer l. Region 0 is free space, so $k_x = k_0 \sin\theta_0$ is real and a constant throughout the stratified medium. However, $k_{lz} = \sqrt{k_l^2 - k_x^2}$ is generally complex. For a stratified medium without other scattering mechanisms (e.g. particle scattering or rough-surface scattering), the solution is expressed entirely in terms of upward- and downward-travelling vertically and horizontally polarized waves. The constants A_l, B_l, C_l and D_l are the

amplitudes of these waves. They are determined by a recurrence relation.

$$\frac{A_l}{B_l}e^{-i2k_{lz}d_l} = \frac{\dfrac{A_{(l+1)}}{B_{(l+1)}}e^{-i2k_{(l+1)z}d_{(l+1)}}}{\dfrac{A_{(l+1)}}{B_{(l+1)}}e^{-i2k_{(l+1)z}d_{(l+1)}}}$$
$$\cdot\frac{e^{i2k_{(l+1)z}(d_{(l+1)}-d_l)} + R_{l(l+1)\mathrm{h}}}{R_{l(l+1)\mathrm{h}}e^{i2k_{(l+1)z}(d_{(l+1)}-d_l)} + 1}. \quad (13)$$

$R_{l(l+1)\mathrm{h}}$ is the Fresnel reflection coefficient for horizontal polarization between regions l and $l + 1$.

$$R_{l(l+1)\mathrm{h}} = \frac{\mu_{(l+1)}k_{lz} - \mu_l k_{(l+1)z}}{\mu_{(l+1)}k_{lz} + \mu_l k_{(l+1)z}}. \quad (14)$$

C_l and D_l satisfy the same recurrence relation as A_l and B_l, except that $R_{l(l+1)\mathrm{h}}$ is replaced by $R_{l(l+1)\mathrm{v}}$ which is the vertically polarized Fresnel reflection coefficient. To obtain $R_{l(l+1)\mathrm{v}}$, replace μ by ϵ in Equation (14).

The brightness temperatures given by Equations (11) and (12) are valid for a single realization of Antarctic firn, a single incident angle, and a single frequency. As discussed earlier, brightness-temperature data are typically spatially averaged over many independent realizations of a stochastic density profile. Furthermore, the bandwidth of a radiometer also introduces some averaging. As long as the ensemble-averaged emission is essentially frequency-independent over the bandwidth of the radiometer, averaging over frequencies is equivalent to averaging over realizations at the center frequency of the radiometer (Carver, 1977). Thus, to compare theoretical results with data, we average computed brightness temperatures from many independent realizations of simulated Antarctic firn.

We neglect contributions to observed brightness temperatures from sky radiation reflected into the radiometer antenna by the firn surface. Such radiation might contribute approximately 5 K to observed brightness temperatures for horizontal polarization and incidence angles $\geq 70°$ (where the firn reflection coefficient would be largest) (Mätzler, 1992). However, we lack data to estimate this effect quantitatively in the present measurements, and therefore do not include it in our model.

Finally, quantitative comparison of the theory with ground-based data requires that we include effects due to the beam pattern and side-lobes of the receiving antenna on the measuring radiometer (henceforth the measurement antenna). The measurement antenna in this study was a pyramidal horn. The measurement-antenna beam-width and side-lobes average emission from a range of directions. We incorporate this effect into the theory by convolving the theoretical results, as functions of incidence angle, with the full beam pattern of the measurement antenna, including side-lobes. We computed the beam-pattern of the measurement antenna using the actual dimensions of the antenna and the theoretical formula for the ideal horn-antenna pattern (Stutzman and Thiele, 1981, ch. 8). As we show in the next section, beam-pattern averaging significantly lowers vertically polarized brightness temperatures at incidence angles of $> 40°$, thus flattening any pronounced Brewster-angle effect in the theoretical emission, because of the entry of radiometrically cold sky radiation through one of the side-lobes.

COMPARISON WITH OBSERVATIONS

In this section we apply the spectral-estimation procedure and scattering theory to four data sets. Three were obtained during an over-snow traverse leading from the coastal station Georg-von-Neumayer to the Heimefront-fjella mountain range during the Antarctic summer of 1989–90. The three sites, designated Veststraumen, Amundsen Ice, and Base Camp, were all at elevations above 500 m and had no indications of melting (Rott and others, 1993b). A fourth data set was collected on the Ronne Ice Shelf during January–February 1992 (Sturm and others, 1992; Rott and others, 1993a).

Veststraumen

The Veststraumen site was located at 74°19.6′ S, 13°44.9′ W at 500 m elevation. The 10 m firn temperature at the site is 253 K, and the surface temperature at the time of the observations in February 1990 was 264 K. The accumulation rate at the site is 260 kg m^{-2} a^{-1} (Rott and others, 1993b).

We have presented the 2.5 m profile of density observations vs depth at this site (Fig. 1), as well as our estimates of the mean density versus depth (Fig. 1) and the spectrum of density fluctuations (Fig. 2), in the process of presenting our model for layered firn and our parameter-estimation procedure. Applying the latter to the characterization data, we estimate the following parameters for the firn at Veststraumen:

$$F(z) = 421 - 206\exp(7.8z),$$
$$\sigma_\mathrm{a} = 39.4\,\mathrm{kg\,m^{-3}},$$
$$\sigma = 49.9\,\mathrm{kg\,m^{-3}},$$
$$\frac{1}{\lambda} = 3.10\,\mathrm{cm}, \quad (15)$$

where z is to be given in meters and $F(z)$ has units of kg m^{-3}. Note that the estimated average layer thickness $(1/\lambda)$ of 3.10 cm is smaller than the 5 cm width of the moving average; the average layer thickness is close to the smallest thickness we could expect to resolve, given the averaging and sampling procedure.

Figures 4 and 5 show 5.25 GHz (6 cm) brightness-temperature observations and model predictions at Veststraumen for vertical and horizontal polarization, respectively, versus incidence angle. Observations are denoted by open circles. The thick solid curves show predictions from our layered-medium emission model using only the parameter estimates in Equation (15) and site-invariant assumptions discussed in the second section. (The dashed curves denote our estimates of confidence intervals for the theoretically predicted emission, to be discussed momentarily.) For comparison, Figures 4 and 5 also plot (as thin solid curves) theoretical brightness temperatures for firn with a temperature profile and mean density profile identical to those at Veststraumen,
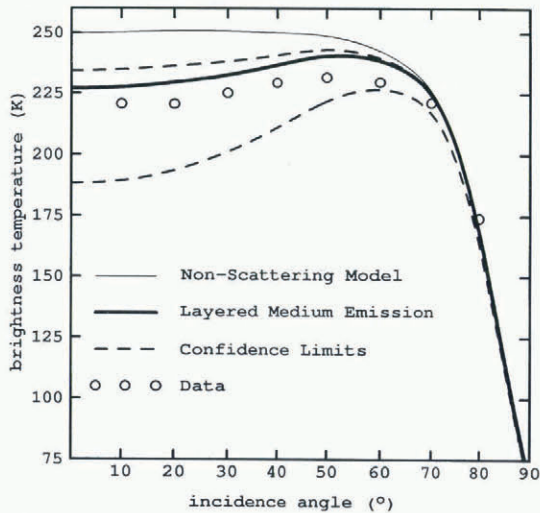
Fig. 4. Vertically polarized brightness temperatures at 6 cm wavelength for Veststraumen. The brightness temperatures for the non-scattering model were computed with the same mean density profile as the layered-medium model. The dashed lines show the range of theoretical brightness-temperature curves associated with the range of λ that lies within a 68% confidence interval about the estimated λ. Temperature profile: $T(z) = 253 + 11\exp(0.4z)$.
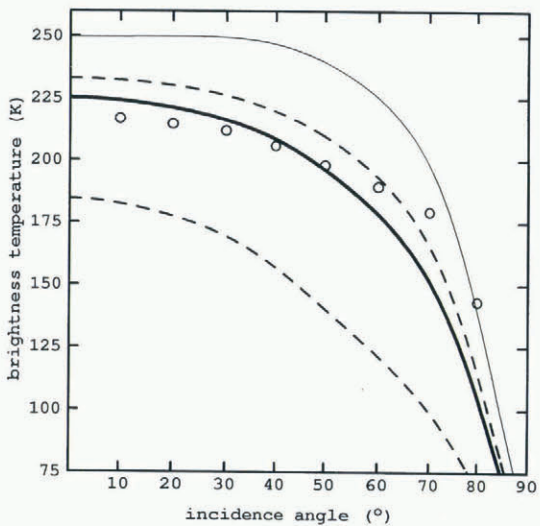

Fig. 5. A comparison of horizontally polarized brightness temperatures at 6 cm wavelength for Veststraumen. (Refer to the legend and caption on Figure 4.)

but assuming no layer-to-layer density variation or other scattering mechanism.

The brightness-temperature observations at Veststraumen are significantly lower than brightness temperatures expected in the absence of scattering. The differences are approximately 22 K (10%) for vertical polarization and 32 K (15%) for horizontal polarization. Thus, the observed polarization contrast (i.e. the difference between emission at vertical and horizontal polarizations) is larger than can be explained by the non-scattering model (or by typical models for scattering from individual ice particles in the firn, such as that of Comiso and others (1982)).

Agreement between observations and predictions from the layered-medium emission model is considerably better. For incidence angles $\leq 40°$, the model predictions agree with observations to within approximately 6 K (3%) for both polarizations; the predictions are offset above the observations by approximately constant amounts over this angular range. At larger incidence angles, the vertically polarized observations rise less near the Brewster angle than do the theoretical predictions, even after accounting theoretically for the effects of the measurement-antenna beamwidth and side-lobes (see previous section). The horizontally polarized observations decline somewhat less rapidly with increasing angle than predicted by the theory (due possibly to our neglect of reflected sky radiation). Thus, the predicted polarization contrast agrees with observations to within approximately 3 K for incidence angles up to 30°, 6 K at 40°, and 11 K at 50°. We note that these results are obtained using only model input parameters that are determined independently, and in most cases objectively, from observations of polar firn.

In assessing the significance of this comparison, it is useful to consider the sensitivities of the signature model and uncertainties in the input parameters. The layered-medium emission theory is most sensitive to variations in λ and σ (and relatively, though not in all cases absolutely, insensitive to the other parameters in the model). The characterization data tightly constrain σ_a and therefore partly constrain σ via Equation (5), but the estimation of λ is, for two reasons, less precise. First, although the fit of our model spectrum to the observations is good (Fig. 2), the quality of this fit is not very sensitive to λ near the best-fit value. This can be understood physically by noting that the best-fit mean layer thickness $(1/\lambda)$ is comparable to the averaging length in the characterization measurements; the averaging process results in the loss of information on the thinner layers that would characterize the layering process more precisely. The result is that our estimate of λ is significantly uncertain. The uncertainty in λ causes a corresponding uncertainty in σ, despite the well-characterized value of σ_a. The second source of uncertainty in λ is the statistical uncertainty in the spectral estimate itself, which is an unavoidable consequence of spectral estimation based on a limited amount of data (Percival and Walden, 1993). The consequence of uncertainty λ is corresponding uncertainty in theoretical predictions of brightness temperature. Note that this type of uncertainty differs from uncertainty due to statistical fluctuation in emission from a statistically homogeneous random medium. As discussed in the previous section, such fluctuations are negligible in most observations due to averaging inherent in the measurement process.

We have estimated the uncertainty in predicted brightness temperatures due to input-parameter uncertainty by means of further Monte Carlo simulation. Specifically, we simulated 1000 2.5 m long realizations of layered-density profiles using our idealized model for the firn and the parameter estimates in Equation (15). We then applied the parameter-fitting procedure to each of these simulated profiles to obtain 1000 sets of parameter estimates in a case with known true parameters. We found little variance in estimates of σ_a (as expected), but

significant variance in estimates of λ and therefore σ. Correlation between the errors in σ_a and λ was small, but errors in λ were highly (positively) correlated with those in σ, as might be expected in light of Equation (5). The observed distributions of λ and σ are non-Gaussian and asymmetric about their means.

We note also that power at low spatial frequencies in the random density-layering process, $X_a(z)$, is difficult to distinguish from variations in the deterministic mean density function, $F(z)$, on long spatial scales. Thus our detrending of the density data may introduce biases into the parameter estimates. In the simulation corresponding to Veststraumen, we observed only small differences between the means of parameter estimates and the parameters used to generate realizations. The potential signature variations due to such biases are small relative to those due to uncertainty (i.e. variance) in the parameter estimates. Simulations corresponding to the other sites discussed below showed that sizes of biases depended on the strength of the variation of mean density with depth; a stronger variation in mean density leads to larger biases. However, at all sites the potential effects of biases remained smaller than those due to parameter uncertainties. We therefore focus here on signature uncertainties due to parameter uncertainties.

Having confirmed that errors in λ and σ are highly correlated, we estimated the uncertainties in predicted brightness temperatures at Veststraumen using the value of σ_a given in Equation (15) and the simulated distribution of λ. We repeated our Monte Carlo signature computations twice, using values of λ corresponding to the 16th and 84th percentile values in the simulated distribution. (The choice of these particular percentile values was somewhat arbitrary, motivated by their correspondence to the percentile values separated by one standard deviation from the mean in the case of a Gaussian distribution.) The signatures corresponding to the 16th percentile λ (i.e. the largest mean layer thickness) are shown as the upper dashed lines in Figures 4 and 5. Those corresponding to the 84th percentile (the smallest mean layer thickness) are shown as the lower dashed lines.

The ranges of uncertainty in predicted brightness temperatures based on the present data are significant. Predicted brightness temperatures could evidently be brought into very close agreement with the observations at incidence angles $\leq 60°$ simply by changing the mean layer thickness in the model to a slightly smaller, only slightly less probable, value.

Note, however, that any such tuning would cause a stronger Brewster-angle effect in the predicted vertically polarized emission, whereas the opposite would be needed to reproduce more accurately the angular dependence of the observations. This discrepancy may be due to our calculation of the effects of measurement-antenna side-lobes on the basis of theoretical formulae (as explained in the previous section). Any departure of the actual measurement antenna from the theoretical ideal would likely result in higher than anticipated side-lobes. The flattening of theoretical results near the Brewster angle is sensitive to the side-lobe level because any sky radiation entering via a side-lobe is radiometrically very cold. Figure 6 illustrates this point with two plots of theoretical
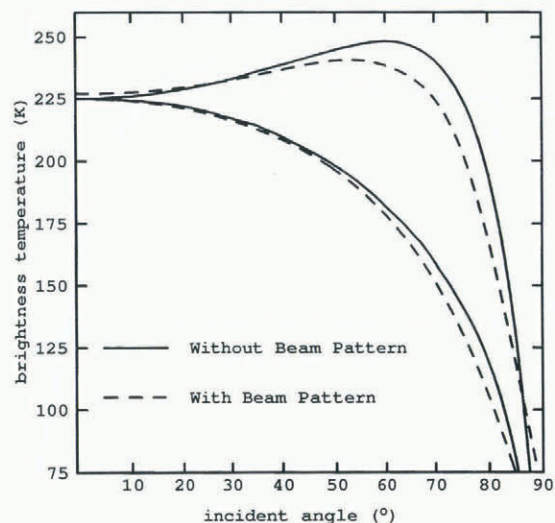

Fig. 6. A comparison between beam-averaged and non-beam-averaged theoretical brightness temperatures at 6 cm wavelength for the layered medium at Veststraumen. Note that the beam pattern separates the vertically and horizontally polarized brightness temperatures at nadir.

brightness temperatures for the Veststraumen site. The solid lines show predictions for vertically and horizontally polarized emission as would be observed using an instrument with effectively infinite directionality (zero beamwidth and side-lobe level). The dashed lines show the corresponding brightness temperatures with our best theoretical accounting for the beam pattern of the measurement antenna used in this study. Even a minor deviation of the actual from the assumed side-lobe level could cause a less pronounced Brewster-angle effect in the theory, similar to that observed.

Finally, we note that the beamwidths and side-lobe corrections in spaceborne radiometers are typically quite different from those in the present ground-based study; readers should therefore take such differences into account when considering the implications of our study for the interpretation of data from such systems.

Amundsen Ice

The Amundsen Ice site was located at $75°33.0'$ S, $10°17.42'$ W, at an elevation of 2250 m. The 10 m firn temperature at this location is 240 K, and the surface temperature at the time of data acquisition was 259 K. The accumulation rate at the site is 130 kg m^{-2} a^{-1} (Rott and others, 1993b). Note that both physical temperatures and the accumulation rate were significantly lower at Amundsen Ice than at Veststraumen. Rott and others (1993b) earlier reported observations of significant hoar layers at several depths at this site.

Figure 7 shows the 2.5 m firn-density profile acquired at this site. In contrast to the Veststraumen site, there is little or no visually apparent trend in mean firn density as a function of depth at this site. This impression is borne out by attempts to fit an exponential profile for mean density to the observations; such attempts fail due to numerical ill-conditioning. We have therefore modelled the mean density as a function of depth at this site as
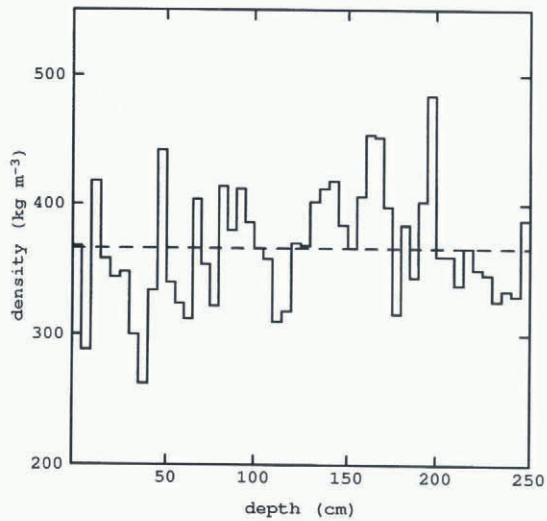
Fig. 7. *The snow-density profile measured at Amundsen Ice (solid line). The profile was obtained by measuring the average density in consecutive 5 cm layers. The dashed line shows the least-squares constant fit to the measured profile. The fitted constant is:* $F(z) = 366 \, kg \, m^{-3}$.

Fig. 8. *Vertically polarized brightness temperatures at 6 cm wavelength for Amundsen Ice. The brightness temperatures for the non-scattering model were computed with the same mean density profile as the layered-medium model. The dashed lines show the range of theoretical brightness-temperature curves associated with the range of λ that lies within a 68% confidence interval about the estimated λ. Temperature profile:* $T(z) = 240 + 19 \exp(0.59z)$.

constant and equal to the mean of the observed density profile, $366 \, \mathrm{kg \, m^{-3}}$.

The other parts of the parameter-estimation procedure can be applied unchanged to this site. We obtained the following parameter estimates:

$$\sigma_a = 45.1 \, \mathrm{kg \, m^{-3}}$$
$$\sigma = 56.1 \, \mathrm{kg \, m^{-3}}$$
$$\frac{1}{\lambda} = 3.38 \, \mathrm{cm} . \tag{16}$$

Note that the estimated average layer thickness differs little from the corresponding value at Veststraumen of 3.10 cm, despite the difference in accumulation rates between the two sites. The standard deviation of density is much greater at this site, as seems consistent with the qualitative observation of depth-hoar layers at Amundsen Ice.

Figures 8 and 9 show brightness-temperature observations and model predictions for vertical and horizontal polarization, respectively, as functions of incidence angle. Vertically and horizontally polarized brightness-temperature observations (open circles) are both considerably lower at Amundsen Ice than at Veststraumen. For vertical polarization, the difference between sites is 23 K at 10° incidence angle, and decreases to 18 K at 50°. The difference at 50° can be ascribed almost entirely to the 14 K lower mean annual temperature at Amundsen Ice. The difference in horizontally polarized emission at the two sites exceeds that for vertical polarization (e.g. 28 K at 50° incidence angle), making the polarization contrast markedly larger at Amundsen Ice. Differences between observations and emission in the absence of scattering (denoted by thin solid lines) are also much larger at this site, e.g. 36 and 53 K for vertical and horizontal polarization, respectively, at 30° incidence angle. All of these observations indicate strong scattering at Amundsen Ice.

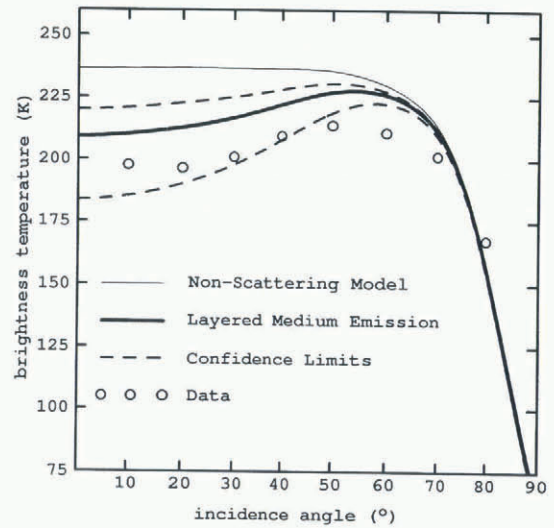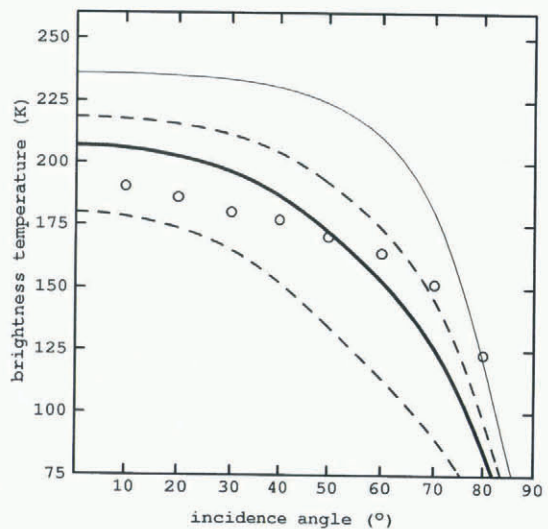The thick solid lines in Figures 8 and 9 show the

Fig. 9. *A comparison of horizontally polarized brightness temperatures at 6 cm wavelength for Amundsen Ice. (Refer to the legend and caption on Figure 8.)*

predictions of the layered-medium emission model, and the dashed lines represent confidence limits, analogous to (and derived via the same procedure as) those given for Veststraumen. Again, all model parameters have been estimated objectively from characterization data or fixed by assumption at site-invariant values. Similar to the situation at Veststraumen, the theoretical predictions are offset above the observations for both polarizations; the offset is larger in this case, approximately 15 K. The computed polarization contrast agrees with the observations to within 5 K for incidence angles ≤40°, but exceeds that observed by 13 K at 50°. As at Veststraumen, these differences are due to a more pronounced Brewster-angle

effect, and a faster decrease in horizontally polarized brightness temperatures with increasing incidence angle, in the theory than is shown in the observations.

At incidence angles of 40° or less, it appears that the discrepancies between theory and observation could again be explained by a mean layer thickness shorter, but not much less probable, than our estimate. At larger incidence angles, inadequate theoretical treatment of measurement-antenna side-lobes may play a role. The theory without antenna-pattern corrections shows a sharper rise and fall of vertically polarized brightness temperatures near the Brewster angle at Amundsen Ice than at Veststraumen. (This occurs because vertically polarized emission at small incidence angles is preferentially lowered by the stronger scattering at this site.) We would therefore expect any error in computing side-lobes effects to be more apparent at Amundsen Ice.

One other potential source of the discrepancy should be considered. The depth-hoar layers reported at this site (Rott and others, 1993b) contained hexagonal ice plates up to 4 mm in diameter which might have caused significant scattering, even at 6 cm wavelength. This type of volume scattering would tend to lower brightness temperatures overall and to reduce the Brewster-angle effect in vertically polarized brightness temperatures (Tsang and others, 1987). However, it would be difficult to explain the observations of large polarization contrast at small incidence angles on the basis of this mechanism alone (unpublished computations by R. West, D. Winebrenner and L. Tsang). It therefore seems likely that its importance to 6 cm emission, if any, is limited to vertical polarization and the angular region near the Brewster angle.

Base Camp

The site Base Camp was located at 74°45.4′ S, 12°23.7′ W, at an elevation of 1200 m. The 10 m firn temperature at this site is 248 K; the surface temperature at the time of data acquisition was 261 K; the accumulation rate is $350 \, \mathrm{kg \, m^{-2} a^{-1}}$. Thus this site is intermediate between Veststraumen and Amundsen Ice geographically and in terms of mean annual temperature, but the accumulation rate is larger, apparently due to its location at the base of a mountain range (Rott and others, 1993b).

Figure 10 shows the measured density profile for Base Camp; at this site, the density profile extends to 3 m depth, and we have used the entire record for parameter estimation, as in our discussion in the second section. Thus, we obtain the following parameter estimates:

$$F(z) = 586 - 195 \exp(0.28z),$$

$$\sigma_{\mathrm{a}} = 2.6 \, \mathrm{kg \, m^{-3}},$$

$$\sigma = 37.7 \, \mathrm{kg \, m^{-3}},$$

$$\frac{1}{\lambda} = 1.16 \, \mathrm{cm}, \tag{17}$$

where, again, z is to be given in meters and the units of $F(z)$ are $\mathrm{kg \, m^{-3}}$. Notice that σ_{a}, the standard deviation of density in the measurements, is considerably smaller at this site than at the previous two. Notice also that the estimated mean layer thickness is considerably smaller as well, and is indeed much smaller than the averaging
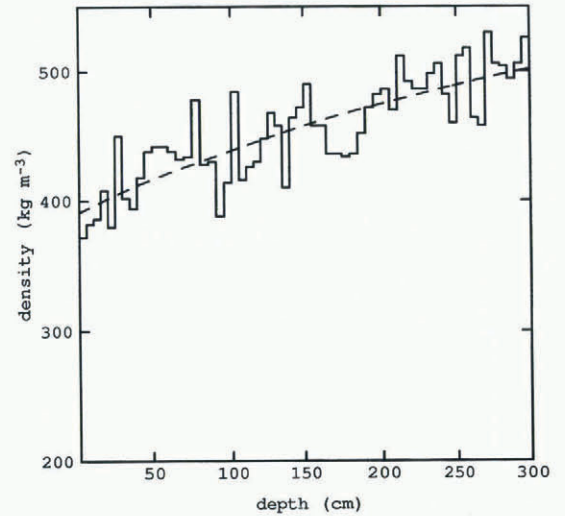

Fig. 10. The snow-density profile measured at Base Camp (solid line). The profile was obtained by measuring the average density in consecutive 5 cm layers. The dashed line shows the least-squares exponential fit to the measured profile. The fitted exponential is: $F(z) = 586 - 195 \exp(0.28z)$ with z a negative value in meters, and $F(z)$ measured in kg m^{-3}.

length in the characterization measurements. This suggests that the estimate of λ at this site is likely to be substantially uncertain.

Examination of the spectrum of detrended density fluctuations confirms this inference. The spectrum, shown in Figure 11, is essentially flat over the range of observable spatial frequencies up to the Nyquist frequency. Model spectra (see Equation (6)) with a range of different λ values fit the observed spectrum almost equally well; the only criterion on the λ values is that they correspond to mean layer thickness much
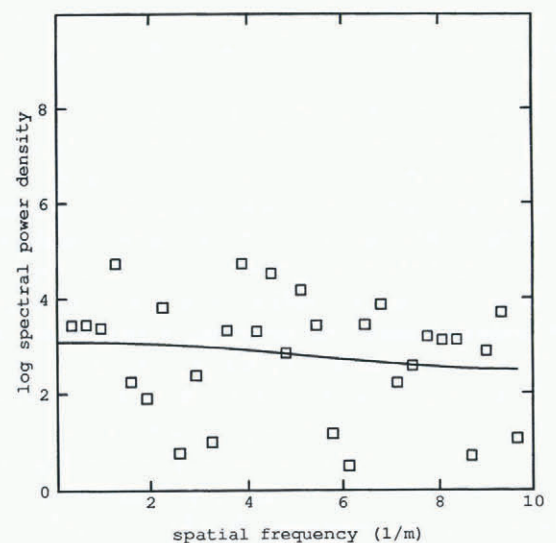

Fig. 11. A comparison between the natural logarithm of the periodogram for the measured density profile at Base Camp (open squares) and the theoretical log spectrum (solid line) fitted in the least-squares sense with $1/\lambda = 1.16 \, cm$, and $\sigma = 37.7 \, kg \, m^{-3}$. The spectrum itself has units of $(kg \, m^{-3})^2 / (1/m)$.

shorter than the averaging length. Whether this situation arises because the true mean layer thickness is very small, or simply because density layering at this site is weak and therefore difficult to characterize, is unclear. In any case, the particular estimate of λ in Equation (17) is highly uncertain. The uncertainties estimated by Monte Carlo simulation in this case are comparable to the parameter estimates themselves. The corresponding uncertainties in predicted brightness temperatures are therefore also large, as we will show momentarily.

The brightness-temperature observations for this site (plotted as open circles in Figures 12 and 13) are slightly higher than those at Veststraumen, despite the fact that mean annual temperature is 5 K lower at this site. The polarization contrast here is smaller than at Veststraumen, and much smaller than at Amundsen Ice. Thus, it appears that scattering at the Base Camp site is weaker than at the other sites, as might be expected given the low value of σ_a at this site. The observations nonetheless fall approximately 13 K below brightness temperatures computed on the basis of no scattering (plotted as thin solid lines in Figures 12 and 13).

The thick solid lines in Figures 12 and 13 show brightness temperatures predicted by the layered-medium emission model based on the parameter estimates in Equation (17). The single dashed line represents the model prediction based on the 16th percentile value in the simulated distribution of λ, which corresponds to a mean layer thickness of 2.10 cm. The plot of brightness
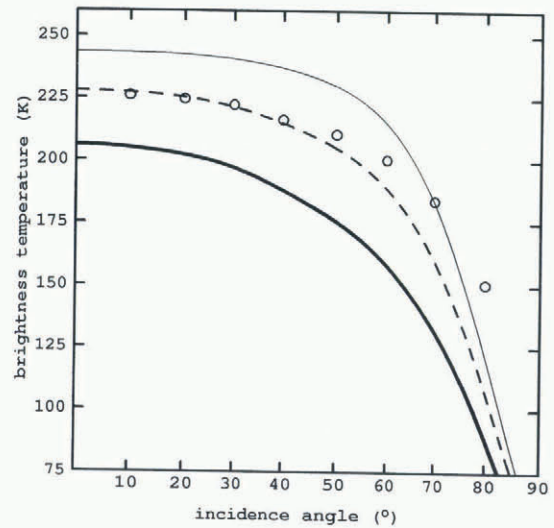

Fig. 13. A comparison of horizontally polarized brightness temperatures at 6 cm wavelength for Base Camp. (Refer to the legend and caption on Figure 12.)

temperatures for the 84th percentile value of λ is so low as to be off the scale of the figures. The mean layer thickness implied by that value of λ is less than a millimeter; we regard such a mean layer thickness as unphysical in view of the size of individual ice grains in firn (roughly 0.5–1 mm). The large uncertainty in λ translates into very large uncertainties in predicted brightness temperatures.

The theoretical predictions based on Equation (17) fall approximately 20 K below the observations at small incidence angles for both polarizations, and show a more pronounced Brewster angle than is observed for vertical polarization. However, brightness-temperature predictions based on the 16th percentile value of λ are slightly above the observations, and display only a slightly greater Brewster-angle effect than that observed. This suggests that the layered-medium emission model can explain the observations at this site as well, and that the discrepancy between the solid line and observations in Figures 12 and 13 is due to the difficulty in accurately estimating the mean layer thickness at this site.

Ronne Ice Shelf

This final comparison involves not a single site but rather a collection of eight sites on the Ronne Ice Shelf between latitudes of approximately 77° and 78°30′ S and longitudes of 62° and 68° W. The data from these sites were acquired during January–February 1992 (Sturm and others, 1992; Rott and others, 1993a). The radiometric observations presented below result from 50 sets of measurements near the eight sites; we therefore present the mean, maximum and minimum brightness temperatures for all observations, at each incidence angle and polarization. Sturm and others (1992) present detailed stratification observations for one of the eight sites (specifically, site 5), including a 5 m profile of density, again averaged in 5 cm increments. We assume here that this profile and other physical properties are representative of the firn at all the sites, and compare brightness-
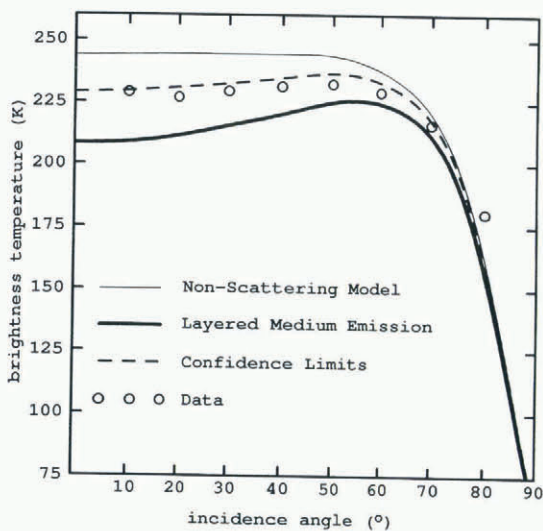

Fig. 12. Vertically polarized brightness temperatures at 6 cm wavelength for Base Camp. The brightness temperatures for the non-scattering model were computed with the same mean density profile as the layered-medium model. The dashed lines show the range of theoretical brightness-temperature curves associated with the range of λ that lies within a 68% confidence interval about the estimated λ. Temperature profile: $T(z) = 248 + 13.3\exp(0.4z)$. The single dashed line represents the model prediction based on the 16th percentile value in the simulated distribution of λ, which corresponds to a mean layer thickness of 2.10 cm. The plot of brightness temperatures for the 84th percentile value of λ is so low as to be off the scale of the figure.

temperature predictions based on those characterization data to the full set of radiometric observations.

The 10 m temperature at the site is 248.5 K, and the surface temperature at the time of data acquisition was approximately 263 K. The accumulation rate, estimated from several data sources, is 161 kg m^{-2} a^{-1}. Figure 14 shows the 5 m density profile for this site; note the apparent decrease in the variance near the bottom of the profile. For this reason, and for consistency with our physical model of the firn, we have used only the upper 4 m of this profile for parameter estimation. Qualitative observations at this site included a number of very thin ice
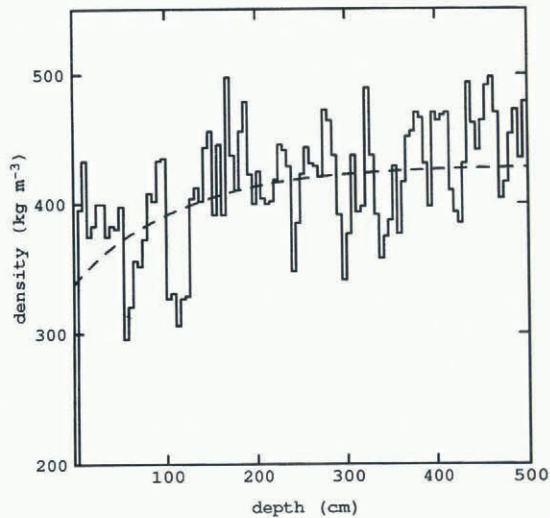

Fig. 14. The snow-density profile measured by Sturm and others (1992) at one location on the Ronne Ice Shelf (solid line). The profile was obtained by measuring the average density in consecutive 5 cm layers. The dashed line shows the least-squares exponential fit to the measured profile (using the top 4 m of data). The fitted exponential is: $F(z) = 429 - 91 \exp(0.88z)$ with z a negative value in meters, and $F(z)$ measured in kg m^{-3}.

crusts and depth-hoar layers (Rott and others, 1993a); thus, there were apparently significant density variations below the scale resolvable with the characterization method, and the observed standard deviation of density is relatively large. Our parameter estimates for this site are

$$F(z) = 429 - 91 \exp(0.88z),$$
$$\sigma_a = 44.4 \, \text{kg m}^{-3},$$
$$\sigma = 58.3 \, \text{kg m}^{-3},$$
$$\frac{1}{\lambda} = 2.62 \, \text{cm}, \tag{18}$$

where again z is to be given in meters and the units of $F(z)$ are kg m^{-3}. The estimated mean layer thickness is again small comparted to the averaging length in the characterization measurements. Though the situation is not quite so problematic as at the Base Camp site, the uncertainties in σ and λ are significantly larger here than at the first two sites, Veststraumen and Amundsen Ice.

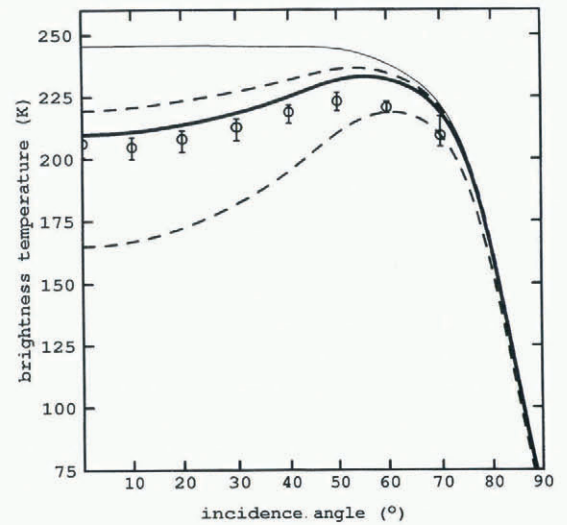Figures 15 and 16 show brightness-temperature

Fig. 15. Vertically polarized brightness temperatures at 6 cm wavelength for the Ronne Ice Shelf. The brightness temperatures for the non-scattering model were computed with the same mean density profile as the layered-medium model. The dashed lines show the range of theoretical brightness-temperature curves associated with the range of λ that lies within a 68% confidence interval about the estimated λ. Temperature profile: $T(z) = 248.5 + 17.5 \exp(0.37z)$.
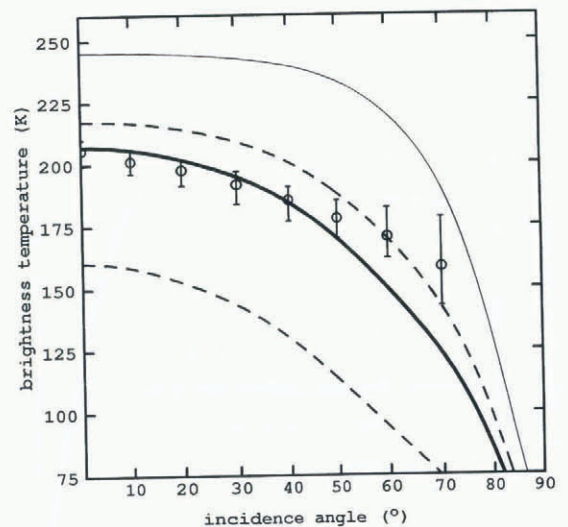

Fig. 16. A comparison of horizontally polarized brightness temperatures at 6 cm wavelength for the Ronne Ice Shelf. (Refer to the legend and caption on Figure 15.)

observations (open circles) and theoretical predictions for this site for vertical and horizontal polarization, respectively. The range of observations at each incidence angle is denoted by a vertical bar. Vertically polarized brightness temperatures at 50° for this site fall 10 K below those at Base Camp, despite a negligible difference in 10 m firn temperatures at the two sites. In contrast, the difference in 10 m firn temperatures between this site and Amundsen Ice matches precisely the difference in vertically polarized brightness temperatures at 50°. The polarization contrast on the Ronne Ice Shelf is also very

similar to that at Amundsen Ice. Brightness temperatures expected in the absence of scattering are roughly 35 K higher than the observations for vertical polarization at this site. The corresponding figure is 45 K higher for horizontal polarization, at incidence angles of roughly 30° or less. Thus, this appears to be a strongly scattering site, somewhat similar to Amundsen Ice.

Predictions from the layered-medium emission model for horizontal polarization (Fig. 18) agree well with observations up to 50° incidence angle, after which the data fall off less rapidly than the theory; this phenomenon is stronger here than at the first three sites. Predictions for vertical polarization fall 5–6 K above the observations for incidence angles ≤40°, and 9 K above at 50°. Again, the ideal horn antenna-pattern correction leads to a somewhat greater Brewster-angle effect in the theoretical predictions than is observed.

CONCLUSIONS

We have compared a model for microwave emission from density-stratified firn at 6 cm wavelength with ground-based emission and characterization measurements, at four disparate sites in Antarctica. According to our model, emission is controlled by scattering from interfaces between firn layers of differing density and thicknesses ranging from a few centimeters down to thin crusts (in addition, of course, to the controlling effect of physical temperature). The model is derived from fluctuation–dissipation theory and the theory of propagation in layered media, and involves averaging over realizations of randomly layered firn. Quantitative comparison with ground-based observations also requires accounting for effects due to the beam pattern and side-lobes of the measurement antenna.

To compare the emission model with observations, we have developed a procedure to estimate model input parameters using the available characterization data. This procedure provides objective estimates of the most sensitive emission-model input parameters; thus our comparisons of theory with data involve no parameter tuning. Note, however, that our parameter estimation procedure is separate from and independent of the emission model itself. Uncertainties, present shortcomings, or future improvements in input parameter estimates will therefore affect signature predictions independently of the merits of the electrodynamic calculations.

The four sites in our study span a significant range in terms of glaciological and radiometric properties. Accumulation rates range from 130 to 350 kg m^{-1} a^{-1}; firn densities at (roughly) 3 m depth range from 366 to 586 kg m^{-1}; and 10 m firn temperatures range from 240 to 253 K. Layer-to-layer density fluctuations were strong at the two low-accumulation-rate, low-density sites (Amundsen Ice and the Ronne Ice Shelf) and weak at the high-accumulation-rate, high-density site (Base Camp). One site (Veststraumen) was intermediate. The Amundsen Ice and Ronne Ice Shelf sites displayed evidence of strong scattering, i.e., brightness temperatures based on a non-scattering model (but with the bulk densities and physical-temperature profiles appropriate to

each site) exceeded those observed by 40–55 K (20–28%), and the observed contrasts between polarizations were much larger than could be explained by such a model. Scattering at the Base Camp site was weaker, though certainly not insignificant, and the Veststraumen site was again intermediate in this regard. We note that these observations are consistent with much larger-scale, though unavoidably less precise, observations by Surdyk and Fily (1993) using satellite-radiometer and historical ground-survey data.

The layered-medium emission model tracks the site-to-site variations well and provides a quantitative physical explanation of the data. Brightness temperatures based on the most probable input parameters (as determined by the characterization data) agree with observations to within 3.5% (8 K) for incidence angles ≤50° at the Veststraumen and Ronne Ice Shelf sites. The standard deviation of random fluctuations in layer density and mean layer thickness most strongly determine the level of scattering in our model. However, these quantities are determined by our estimation procedure only to within substantial uncertainties, due to the unavoidably limited length and depth resolution of the density characterization. Thus, values of sensitive input parameters within significant ranges are only slightly less probable than the most probable values, given the available characterization data. The ranges of corresponding brightness-temperature predictions are therefore also significant. The agreements between observations and theoretical predictions based on the most probable input parameters at Amundsen Ice (15 K, or 7.5%) and Base Camp (22 K, or 10%) should be assessed in this light. Estimation of the mean layer thickness for the Base Camp site was especially problematic. In both these cases, input parameters only slightly less probable than the most probable values lead to very good agreement between theory and data away from the Brewster angle. Small additional discrepancies near the Brewster angle (at all sites) may well be due to inadequate accounting for actual antenna side-lobe effects, as opposed to the correction for an ideal antenna assumed in our calculations.

Thus, to within the present uncertainties in model input parameters, the layered-emission model is capable of explaining 6 cm wavelength radiometric variability at four substantially differing sites and, by implication, over larger areas of polar firn. It should be noted, however, that the present study cannot rule out the possible significance of other scattering mechanisms (e.g. volume scattering from depth-hoar crystals) in at least some situations. Therefore, the most obvious further research called for is studies similar to that reported here but involving finer depth resolution in density-characterization records and coincident, quantitative grain-size information.

Desirable further work notwithstanding, our present results contribute to efforts to estimate glaciological variables remotely from microwave observations. Because long-wavelength (4.5–6 cm), dual-polarization emission observations can be quantitatively related to the 10 m firn temperature and layering parameters, such observations may, in principle, be used to estimate 10 m firn temperatures over wide areas of the dry-snow zones of

Antarctica and Greenland. We will present a physically based algorithm to do so, together with tests against independent temperature data, in a forthcoming study.

ACKNOWLEDGEMENTS

REFERENCES

Alley, R. B. 1988. Concerning the deposition and diagenesis of strata in polar firn. *J. Glaciol.*, **34**(118), 283–290.

Benson, C. S. 1959. Physical investigations on the snow and firn of northwest Greenland during 1952, 1953, and 1954. *SIPRE Res. Rep.* 26.

Callen, H. B. and T. A. Welton. 1951. Irreversibility and generalized noise. *Phys. Rev.*, **83**(1), 34–40.

Carver, K. R. 1977. Radiometric recognition of coherence. *Radio Sci.*, **12**(3), 371–379.

Comiso, J. C., H. J. Zwally and J. L. Saba. 1982. Radiative transfer modeling of microwave emission and dependence on firn properties. *Ann. Glaciol.*, **3**, 54–58.

Fily, M. and J.-P. Benoist. 1991. Large-scale statistical study of Scanning Multichannel Microwave Radiometer (SMMR) data over Antarctica. *J. Glaciol.*, **37**(125), 129–139.

Gow, A. J. 1968. Deep core studies of the accumulation and densification of snow at Byrd Station and Little America V, Antarctica, Greenland. *CRREL Res. Rep.* 197.

Klyatskin, V. I. and V. I. Tatarskii. 1977. Statistical theory of wave propagation through random layered media. *Radiophys. Quantum Electron.* (Engl. Transl.), **20**(7), 720–729.

Landau, L. D. and E. M. Lifshitz. 1960. *Electrodynamics of continuous media.* New York, etc., Pergamon Press. (Course of theoretical physics 8.)

Mätzler, C. 1987. Applications of the interaction of microwaves with the natural snow cover. *Remote Sensing Rev.*, **2**(2), 259–387.

Mätzler, C. 1992. Ground-based observations of atmospheric radiation at 5, 10, 21, 35, and 94 GHz. *Radio Sci.*, **27**(3), 403–415.

Papoulis, A. 1991. *Probability, random variables, and stochastic processes. Third edition.* New York, etc., McGraw-Hill.

Percival, D. and A. Walden. 1993. *Spectral analysis for physical applications.* Cambridge, etc., Cambridge University Press.

Rotman, S. R., A. D. Fisher and D. H. Staelin. 1982. Inversion for physical characteristics of snow using passive radiometric observations. *J. Glaciol.*, **28**(98), 179–185.

Rott, H., K. Sturm and H. Miller. 1993a. Active and passive microwave signatures of Antarctic firn by means of field measurements and satellite data. *Ann. Glaciol.*, **17**, 337–343.

Rott, H., K. Sturm and H. Miller. 1993b. Signatures of Antarctic firn by means of ERS-1 AMI and by field measurements. *In* Kaldeich, B., *ed. Proceedings of the First ERS-1 Symposium: Space at the Service of our Environment, 4–6 November 1992, Cannes, France. Vol. 1.* Paris, European Space Agency, 227–233. (ESA SP-359.)

Shuman, C. A., R. B. Alley and S. Anandakrishnan. 1993. Characterization of a hoar-development episode using SSM/I brightness temperatures in the vicinity of the GISP2 site, Greenland. *Ann. Glaciol.*, **17**, 183–188.

Sturm, K., J. L. Bamber, H. Oerter, H. Miller and H. Rott. 1992. Glaciological fieldwork on the Ronne Ice Shelf with the ERS-1 field campaign 1992. *In* Oerter, H., *ed. Filchner-Ronne Ice Shelf Programme. Report No.6.* Bremerhaven, Alfred-Wegener-Institute for Polar and Marine Research, 74–82.

Stutzman, W. L. and G. A. Thiele. 1981. *Antenna theory and design.* New York, etc., John Wiley and Sons.

Surdyk, S. and M. Fily. 1993. Comparison of the passive microwave spectral signature of the Antarctic ice sheet with ground traverse data. *Ann. Glaciol.*, **17**, 161–166.

Tsang, L., J. A. Kong and R. T. Shin. 1987. *Theory of microwave remote sensing.* New York, etc., John Wiley and Sons.

Zwally, H. J. 1977. Microwave emissivity and accumulation rate of polar firn. *J. Glaciol.*, **18**(79), 195–215.